ChemComm

RSC Publishing

COMMUNICATION

View Article Online
View Journal | View Issue

Stimuli-responsive plasmonic core–satellite assemblies: i-motif DNA linker enabled intracellular pH sensing†

Cite this: *Chem. Commun.*, 2013, **49**, 5739

Received 14th March 2013,
Accepted 15th April 2013

DOI: 10.1039/c3cc80005a

www.rsc.org/chemcomm

Chenxu Wang,‡[a] Yan Du,‡[a] Qiong Wu,[b] Shuguang Xuan,[b] Jiajing Zhou,[a] Jibin Song,[a] Fangwei Shao*[b] and Hongwei Duan*[a]

We report stimuli-responsive core–satellite assemblies of binary gold nanoparticles, linked by i-motif DNA, for live cell plasmonic imaging of pH changes in the endocytic pathway.

Localized surface plasmon resonance (LSPR), originating from the collective oscillation of free conduction electrons, plays a dominant role in shaping the optical properties of metal nanostructures.[1] The dependence of LSPR on the intrinsic properties (size, shape, and chemical composition) of plasmonic nanomaterials and their immediate external environment forms the fundamental basis of metal nanostructure based sensing devices. In particular, the characteristic spectral red-shifts of LSPR, induced by plasmon coupling of neighboring nanoparticles in close proximity, have stimulated considerable research efforts in target-specific self-assembly of plasmonic nanostructures, leading to colorimetric sensors for a wide spectrum of biological and environmental targets.[2] While early efforts mainly afforded irregular macroscopic aggregates, the recent development has shown a paradigm shift toward well-defined plasmonic assemblies with molecular-like structures.[3] The resultant discrete assemblies of plasmonic nanoparticles not only show addressable optical signatures but also offer the possibility to overcome size-limitations in biological barriers such as cellular uptake and tumor targeting when used in living systems.[4]

A layer of ''soft corona'' is often necessitated to direct the self-assembly of the ''hard'' inorganic cores by imparting specific recognition to the nanoparticles. Functional coatings that allow for biologically triggered transition between the well-defined assemblies and their building blocks are of particular interest because the distinct change in plasmonic properties during the transition provides a new means to monitor dynamic molecular and cellular processes, which is traditionally attained by fluorescent resonance energy transfer (FRET).[5] Unlike fluorescence probes such as small molecular dyes, fluorescent proteins, and semiconductor quantum dots, plasmonic nanostructures exhibit photobleaching-free and consistent scattering signals at their LSPR wavelengths that are readily detectable using dark-field microscopy at the single-particle level. In combination with controlled self-assembly, plasmonic imaging has emerged as a powerful technique for imaging and spectroscopic detection in live cells.[4,5]

Among the diverse collections of functional coatings for surface engineering of plasmonic nanostructures, DNA has become the top candidate because of its programmable sequence and base-pairing properties. Significant progress has been made in developing Au–DNA hybrid nanostructures, with DNA attached to the nanoparticles through the Au–S bond or non-covalent interactions.[6] The base-pairing-driven assembly of Au nanoparticles (AuNPs) has been explored to design sensors for nucleic-acid-associated targets such as single-base-pair mismatch and DNA methylation.[7] Recently, the discovery of DNA structures such as aptamers and quadruplexes has greatly diversified the potential targets of interest. Consequently, plasmonic DNA nanostructures have found widespread use in diagnostics, food safety, and environmental screening.[8]

We here present the development of stimuli-responsive core–satellite assembly of binary AuNPs bridged by i-motif DNA linkers and its use for pH sensing in live cells, as illustrated in Fig. 1. Acidification is associated with a number of physiological and pathological processes, and has raised considerable research interest in developing molecular and nanoscale sensors for pH analysis at cellular levels.[9,10] The multiple stretches of cytosine in i-motif DNA are partially protonated under acidic conditions (pH 5.0), giving rise to $C:C^+$ base pairing that drives the single-stranded DNA (ssDNA) to fold into a quadruplex.[11] This pH-triggered conformational change in i-motif DNA has been used to modulate the assembly of AuNPs by pH changes.[12] However, the existing studies mostly led to disordered macroscopic aggregates of AuNPs,[12]

[a] *School of Chemical and Biomedical Engineering, Nanyang Technological University, 70 Nanyang Drive, Singapore 637457. E-mail: hduan@ntu.edu.sg*
[b] *School of Physical and Mathematical Sciences, Nanyang Technological University, 21 Nanyang Link, Singapore 637371. E-mail: fwshao@ntu.edu.sg*

† Electronic supplementary information (ESI) available. See DOI: 10.1039/c3cc80005a

‡ Chenxu Wang and Yan Du contributed equally to this work.

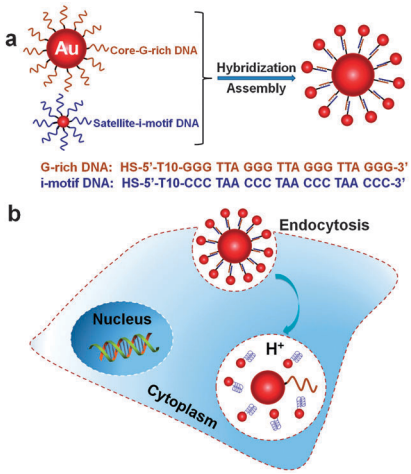

Fig. 1 Schematic illustration of the formation (a) and pH-triggered intracellular disassembly of the core–satellite nanostructure (CSNS) of DNA-functionalized 50 nm core and 14 nm satellite AuNPs (b).

which were not possible to be deployed in living systems as miniature sensors. One key finding of the current work is that well-defined core–satellite assembly of two different sized AuNPs can be constructed by tailoring the sequence and loading of complementary ssDNA on the two sets of AuNPs and the ratio of core and satellite AuNPs.

The "satellite" AuNPs of 14 nm with i-motif ssDNA attached through the Au–S bond were assembled with the 50 nm "core" AuNPs carrying the guanine (G)-rich ssDNA (the complementary strand of i-motif DNA) (Fig. 1a) to form the core–satellite nanostructures (CSNSs). Fig. 2a shows that LSPR of the assembly formed at a feeding core–satellite ratio of 1 : 200 exhibited a red-shift of 14 nm relative to that of the core AuNPs. While spectral properties of the CSNSs showed long-term stability at pH 8.0 (Fig. S1, ESI†), the red-shift disappeared at pH 5.0, with a sharp blue-shift in the pH range of 5.0–6.0 (Fig. S2, ESI†).

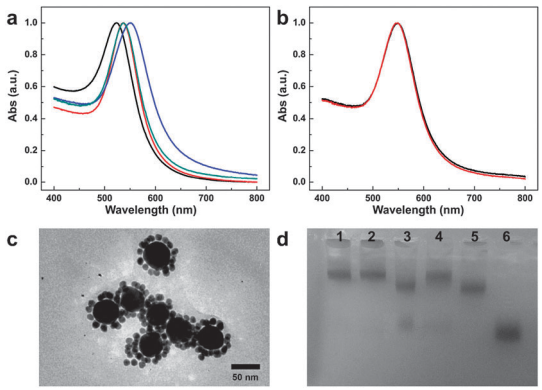

Fig. 2 (a) UV-vis spectra of DNA functionalized AuNPs and CSNSs: 14 nm satellite AuNPs (black line), 50 nm core AuNPs (red line), CSNSs at pH 8.3 (blue line) and disassembled CSNSs at pH 5.0 (green line). (b) UV-vis spectra of CSNSs formed through the hybridization of pH-insensitive control DNA strands: at pH 8.3 (black line) and at pH 5.0 (red line). (c) TEM image of the CSNSs. (d) Electrophoretic analysis of AuNPs and CSNSs: lane 1: control sample at pH 5.0; lane 2: control sample at pH 8.3; lane 3: i-motif CSNSs at pH 5.0; lane 4: i-motif CSNSs at pH 8.3; lane 5: 50 nm AuNPs; lane 6: 14 nm AuNPs.

Apparently, the complementary recognition of the ssDNAs and the pH sensitive folding of i-motif DNA into a closed quadruplex were retained when grafted onto AuNPs. The conformational change in i-motif DNA releases the "satellite" AuNPs from the "cores", leading to reduced interparticle plasmonic coupling. In contrast, assembled structures directed by a control DNA lacking the i-motif sequence did not show the pH sensitivity (Fig. 2b). TEM observation clearly displayed well-defined CSNSs, which have an average number of ~40 satellites per 50 nm core (ESI†). We also used gel electrophoresis to investigate the assembly and disassembly of our CSNSs (Fig. 2d). The CSNSs of larger sizes migrate slower than the building blocks in the gel. And the i-motif CSNSs treated with pH 5.0 buffer clearly gave rise to two bands corresponding to the "core" and "satellite" AuNPs. Consistent with the UV-vis results, the CSNSs built upon the control pH-insensitive ssDNA did not show changes at acidic pH.

We have found that the formation of well-defined CSNSs is highly dependent on the relative ratio of the core and satellite AuNPs. At a low ratio of 1 : 20, the LSPR red-shifted to 589 nm, suggesting stronger plasmonic coupling. Increasing the ratio up to 1 : 300 resulted in a gradual shift in the LSPR to shorter wavelengths, which became stable at a ratio of 1 : 200 (Fig. S3, ESI†). Obviously, at the low ratios, the limited number of "satellite" AuNPs has a higher possibility of interacting with multiple cores to afford large aggregates. Correspondingly, higher ratios are favourable for the formation of well-defined CSNSs, because the crowding satellite particles would have little chance to be linked to the same "core" AuNPs. Since the G-rich ssDNA on the 50 nm "core" tends to form a G-quadruplex in the presence of K^+ ions, which are abundant in an intracellular environment, we also examined the stability of the i-motif CSNSs against K^+ ions. The LSPR of the i-motif CSNSs did not show any response to K^+ of 110 mM. We reason that the large ratio of the i-motif DNA to the G-rich ssDNA resulting from the core–satellite construct contributes to the stability observed here. This is supported by the fact that loading the i-motif on the core and G-rich ssDNA on the satellite gave rise to CSNSs sensitive to both pH and K^+ (Fig. S5–S9, ESI†).

The well-defined CSNSs offer the possibility of monitoring their pH-triggered disassembly at the single-particle level. The 50 nm "core" AuNPs exhibit distinct green scattering light (Fig. S10, ESI†). And the 14 nm "satellite" AuNPs have negligible scattering and therefore are invisible under a dark-field microscope. As shown in Fig. 3a, the attachment of multiple 14 nm AuNPs on the 50 nm "core" AuNPs led to CSNSs with bright yellow scattering light, resulting from the red-shift of the scattering light (Fig. 3c) due to interparticle coupling. Consistent with the bulk assay detected by UV-vis spectra, the color of the i-motif CSNSs turned into green and scattering spectra showed a blue-shift of 17 nm, confirming the possibility of using the CSNSs as miniature pH sensors. The CSNSs assembled by control DNA sequences showed similar yellow scattering light, but no color change in scattering light was observed when tuning pH of the solution to 5.0 (Fig. 3b). Similarly, the scattering spectrum of representative control

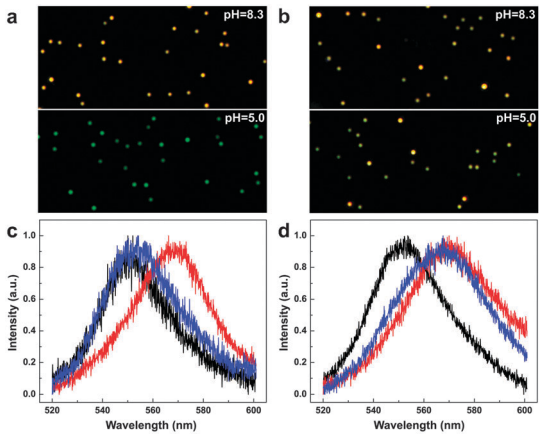

Fig. 3 (a and b) Dark field images of i-motif (a) and control CSNSs (b). Upper: pH 8.3. Lower: pH 5.0. (c and d) Scattering spectra of i-motif (c) and control (d) CSNSs: core AuNPs (50 nm) (black line), CSNSs at pH 8.3 (red line) and pH 5.0 (blue line).

CSNSs showed hardly any difference at pH 8.3 and pH 5.0 (Fig. 3d).

We next investigated the use of i-motif CSNSs to detect the pH variation in live cells once they are uptaken through endocytosis. The compact size of the CSNSs of 90–100 nm allows for efficient uptake by macrophage cells (RAW 264.7 cells) upon incubation for 15 min (Fig. 4a). Within 30 min, the yellow scattering signal from CSNSs in the cells mostly became green, suggesting the disassembly of CSNSs into elementary units inside acidic intracellular compartments (Fig. 4b). Spectral blue-shifts revealed by scattering spectra (Fig. S11, ESI†) are in line with the observed color change. It is well-known that pH in the endocytic pathway drops from 5.9–6.2 in early endosomes to 4.7–5.5 in late endosomes/lysosomes, which agrees well with our imaging results.[9] Plasmonic imaging also suggests that the DNA-functionalized AuNPs maintained excellent colloidal stability in the acidic organelles. This is critical for the plasmonic imaging based on the CSNS assembly, because aggregation of AuNPs would lead to red-shifts of the scattering light and generate false imaging signals. In clear contrast, pH-insensitive control CSNSs showed no obvious color change in the same time scale (Fig. 4c–d), although they can also be efficiently uptaken by the cell. Cytotoxicity tests show that the cells treated with CSNSs are well spread with viabilities of more than 90% (Fig. S12, ESI†). To confirm the mechanism of cellular entry of the CSNSs, the nanostructures were incubated with macrophages at 4 °C, under which the rigid cell membrane can block the non-specific endocytosis uptake of CSNSs by macrophage cells.[9] Consistently, the dark field image showed greatly reduced cellular uptake of CSNSs at 4 °C (Fig. S13, ESI†).

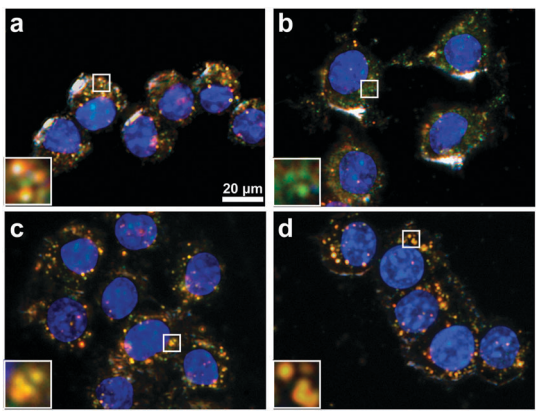

Fig. 4 Overlaid dark field and fluorescence images of cells incubated with i-motif (a, b) and control (c, d) CSNSs after 15 min incubation (a, c) and 30 min post-incubation (b, d). Insets show magnified images of the specific framed areas. Cell nuclei were stained with blue fluorescent Hoechst 33342.

In summary, we have reported a new class of well-defined core–satellite plasmonic assembly of binary AuNPs, with pH-responsive disassembly enabled by an i-motif DNA linker. Our results have shown that the i-motif CSNSs undergo endocytosis when cultured with macrophage cells and allow for plasmonic imaging of pH changes in the endocytic pathway in live cells. This concept of constructing CSNSs and the expanded library of stimuli-responsive DNA provides new opportunities to develop miniature plasmonic sensors for a diverse range of targets. The introduction of targeting ligands to recognize specific cell types, in combination with techniques for intracellular delivery of the plasmonic assembly, would further broaden their use for intracellular detection.

The authors thank the financial support by Nanyang Assistant Professorship and the INSIST programs.

Notes and references

1 P. K. Jain, X. Huang, I. H. El-Sayed and M. A. El-Sayed, *Acc. Chem. Res.*, 2008, **41**, 1578.
2 (*a*) J. I. Cutler, E. Auyeung and C. A. Mirkin, *J. Am. Chem. Soc.*, 2012, **134**, 1376; (*b*) M. Grzelczak, J. Vermant, E. M. Furst and L. M. Liz-Marzan, *ACS Nano*, 2010, **4**, 3591; (*c*) Y. Wang, J. Xu, Y. Wang and H. Chen, *Chem. Soc. Rev.*, 2013, **42**, 2930.
3 M. P. Busson, B. Rolly, B. Stout, N. Bonod, E. Larquet, A. Polman and S. Bidault, *Nano Lett.*, 2011, **11**, 5060.
4 (*a*) J. Song, L. Cheng, A. Liu, J. Yin, M. Kuang and H. Duan, *J. Am. Chem. Soc.*, 2011, **133**, 10760; (*b*) J. Song, J. Zhou and H. Duan, *J. Am. Chem. Soc.*, 2012, **134**, 13458.
5 (*a*) J. N. Anker, W. P. Hall, O. Lyandres, N. C. Shah, J. Zhao and R. P. Van Duyne, *Nat. Mater.*, 2008, **7**, 442; (*b*) J. Wang, S. V. Boriskina, H. Y. Wang and B. M. Reinhard, *ACS Nano*, 2011, **5**, 6619.
6 (*a*) S. J. Hurst, A. K. Lytton-Jean and C. A. Mirkin, *Anal. Chem.*, 2006, **78**, 8313; (*b*) H. Pei, F. Li, Y. Wan, M. Wei, H. Liu, Y. Su, N. Chen, Q. Huang and C. Fan, *J. Am. Chem. Soc.*, 2012, **134**, 11876; (*c*) S. J. Tan, M. J. Campolongo, D. Luo and W. L. Cheng, *Nat. Nanotechnol.*, 2011, **6**, 268.
7 (*a*) R. Elghanian, J. J. Storhoff, R. C. Mucic, R. L. Letsinger and C. A. Mirkin, *Science*, 1997, **277**, 1078; (*b*) T. Liu, J. Zhao, D. M. Zhang and G. X. Li, *Anal. Chem.*, 2010, **82**, 229.
8 L. Xu, H. Kuang, C. Xu, W. Ma, L. Wang and N. A. Kotov, *J. Am. Chem. Soc.*, 2012, **134**, 1699.
9 (*a*) K. Zhou, H. Liu, S. Zhang, X. Huang, Y. Wang, G. Huang, B. D. Sumer and J. Gao, *J. Am. Chem. Soc.*, 2012, **134**, 7803; (*b*) A. Pallaoro, G. B. Braun, N. O. Reich and M. Moskovits, *Small*, 2010, **6**, 618.
10 (*a*) X. G. Hu and X. H. Gao, *ACS Nano*, 2010, **4**, 6080; (*b*) P. T. Snee, R. C. Somers, G. Nair, J. P. Zimmer, M. G. Bawendi and D. G. Nocera, *J. Am. Chem. Soc.*, 2006, **128**, 13320.
11 C. H. Kang, I. Berger, C. Lockshin, R. Ratliff, R. Moyzis and A. Rich, *Proc. Natl. Acad. Sci. U. S. A.*, 1994, **91**, 11636.
12 (*a*) Y. Zhao, L. Cao, J. Ouyang, M. Wang, K. Wang and X. H. Xia, *Anal. Chem.*, 2013, **85**, 1053; (*b*) J. Sharma, R. Chhabra, H. Yan and Y. Liu, *Chem. Commun.*, 2007, 477.